

LETTER TO THE EDITOR

# The importance of radiative pumping on the emission of the H<sub>2</sub>O submillimeter lines in galaxies

Eduardo González-Alfonso<sup>1</sup>, Jacqueline Fischer<sup>2</sup>, Javier R. Goicoechea<sup>3</sup>, Chentao Yang<sup>4</sup>, Miguel Pereira-Santaella<sup>5</sup>, and Kenneth P. Stewart<sup>2</sup>

<sup>1</sup> Universidad de Alcalá, Departamento de Física y Matemáticas, Campus Universitario, E-28871 Alcalá de Henares, Madrid, Spain  
e-mail: eduardo.gonzalez@uah.es

<sup>2</sup> George Mason University, Department of Physics & Astronomy, MS 3F3, 4400 University Drive, Fairfax, VA 22030, USA

<sup>3</sup> Instituto de Física Fundamental (IFF), CSIC. Calle Serrano 121-123, 28006, Madrid, Spain

<sup>4</sup> Department of Earth and Space Sciences, Chalmers University of Technology, Onsala Observatory, 439 94 Onsala, Sweden

<sup>5</sup> Centro de Astrobiología (CSIC-INTA), Ctra. de Ajalvir, km. 4, 28850 Torrejón de Ardoz, Madrid, Spain

September 15, 2022

## ABSTRACT

H<sub>2</sub>O submillimeter emission is a powerful diagnostic of the molecular interstellar medium in a variety of sources, including low- and high-mass star forming regions of the Milky Way, and from local to high redshift galaxies. However, the excitation mechanism of these lines in galaxies has been debated, preventing a basic consensus on the physical information that H<sub>2</sub>O provides. Both radiative pumping due to H<sub>2</sub>O absorption of far-infrared photons emitted by dust and collisional excitation in dense shocked gas have been proposed to explain the H<sub>2</sub>O emission. Here we propose two basic diagnostics to distinguish between the two mechanisms: 1) in shock excited regions, the ortho-H<sub>2</sub>O 3<sub>21</sub> – 2<sub>12</sub> 75 μm and the para-H<sub>2</sub>O 2<sub>20</sub> – 1<sub>11</sub> 101 μm rotational lines are expected to be in emission while, if radiative pumping dominates, both far-infrared lines are expected to be in absorption; 2) based on statistical equilibrium of H<sub>2</sub>O level populations, the radiative pumping scenario predicts that the apparent isotropic net rate of far-infrared absorption in the 3<sub>21</sub> ← 2<sub>12</sub> (75 μm) and 2<sub>20</sub> ← 1<sub>11</sub> (101 μm) lines should be higher than or equal to the apparent isotropic net rate of submillimeter emission in the 3<sub>21</sub> → 3<sub>12</sub> (1163 GHz) and 2<sub>20</sub> → 2<sub>11</sub> (1229 GHz) lines, respectively. Applying both criteria to all 16 galaxies and several galactic high-mass star-forming regions where the H<sub>2</sub>O 75 μm and submillimeter lines have been observed with *Herschel*/PACS and SPIRE, we show that in most (extra)galactic sources the H<sub>2</sub>O submillimeter line excitation is dominated by far-infrared pumping, with collisional excitation of the low-excitation levels in some of them. Based on this finding, we revisit the interpretation of the correlation between the luminosity of the H<sub>2</sub>O 988 GHz line and the source luminosity in the combined galactic and extragalactic sample.

**Key words.** Galaxies: evolution – Galaxies: nuclei – Infrared: galaxies – Submillimeter: galaxies

## 1. Introduction

Soon after the launch of the *Herschel Space Observatory* (Pilbratt et al. 2010), spectroscopic observations with the SPIRE instrument (Griffin et al. 2010) revealed strong H<sub>2</sub>O submillimeter (hereafter submm) emission from the ultraluminous infrared galaxy (ULIRG) Mrk 231, with strengths comparable to the those of the CO lines (van der Werf et al. 2010). The H<sub>2</sub>O submm lines were subsequently detected in a variety of local galaxies with SPIRE (see Yang et al. 2013; Lu et al. 2017, and references therein) and also HIFI (Liu et al. 2017), as well as in high-redshift ULIRGs and Hyper-LIRGs from ground based facilities (e.g. Omont et al. 2011, 2013; van der Werf et al. 2011; Yang et al. 2016, 2019). Based on the H<sub>2</sub>O line fluxes in galaxies at all redshifts, Omont et al. (2013) and Yang et al. (2013) found a strong correlation between the H<sub>2</sub>O line luminosities and the infrared luminosities of the galaxies,  $L_{\text{H}_2\text{O-submm}} \propto L_{\text{IR}}^\alpha$ , with an index  $\alpha$  slightly higher than unity. The extragalactic H<sub>2</sub>O submm emission has been modeled in terms of radiative pumping (González-Alfonso et al. 2010, 2014, 2021; Pereira-Santaella et al. 2017), and the  $L_{\text{H}_2\text{O-submm}} - L_{\text{IR}}$  correlations appeared to support this view (Omont et al. 2013; Yang et al. 2013; Lu et al. 2017).

In parallel, several H<sub>2</sub>O submm lines have been observed in a large number of both low-mass and high-mass star-forming regions (LMSFR and HMSFRs) in our galaxy (e.g. van Dishoeck et al. 2021, and references therein) with the HIFI instrument (de Graauw et al. 2010). The lines were resolved with the high spectral resolution provided by HIFI, showing broad profiles characteristic of outflows and their associated dense shocked gas where the H<sub>2</sub>O submm emission is collisionally excited. The H<sub>2</sub>O line profiles also often showed a narrower spike at central velocities, which contributes negligibly (often in absorption) to the integrated emission in LMSFRs (e.g. Kristensen et al. 2012), but accounts for an average of ~ 40% in HMSFRs (San José-García et al. 2016) and is attributed to the warm, massive envelopes around the luminosity sources. Considering both galactic and extragalactic sources, San José-García et al. (2016) found a strong  $L_{\text{H}_2\text{O-submm}} - L_{\text{IR}}$  correlation with an index  $\alpha$  that was higher (and closer to unity) than when only the galactic sources were fitted.

Using *Infrared Space Observatory* (ISO, Kessler et al. 1996) data (with 80'' aperture) and radiative transfer models, Cernicharo et al. (2006) found that much of the H<sub>2</sub>O line excitation in the Orion KL outflow is driven by the dust continuum radiation. On the other hand, van Dishoeck et al. (2021) argued, based on the nearly linear ( $\alpha = 0.95 \pm 0.02$ ) correlation they found be-

tween *Herschel* H<sub>2</sub>O 2<sub>02</sub> – 1<sub>11</sub> 988 GHz line luminosities of both galactic and extragalactic sources versus source luminosity, that the H<sub>2</sub>O submm emission in galaxies may be a scaled-up version of galactic sources, where the  $L_{\text{H}_2\text{O-submm}} - L_{\text{IR}}$  correlation is set by H<sub>2</sub>O collisional excitation in dense shocks.

In this Letter we address this lack of consensus on the excitation mechanism of these lines in galaxies, and thus on the physical information that H<sub>2</sub>O provides on the sources from which the H<sub>2</sub>O emission lines arise. We propose both a qualitative and a quantitative diagnostic to distinguish between the two mechanisms, each involving the far-infrared (far-IR) H<sub>2</sub>O 3<sub>21</sub> – 2<sub>12</sub> 75  $\mu\text{m}$  and 2<sub>20</sub> – 1<sub>11</sub> 101  $\mu\text{m}$  lines, and apply them to all extragalactic sources and a sample of HMSFRs where the H<sub>2</sub>O 75  $\mu\text{m}$  and 1163 GHz lines have been observed with *Herschel*/PACS (Poglitsch et al. 2010) and SPIRE, respectively. A flat  $\Lambda$ CDM cosmology with  $H_0 = 70 \text{ km s}^{-1} \text{ Mpc}^{-1}$  and  $\Omega_M = 0.27$  is adopted, but for some nearby galaxies preferred distances are used.

## 2. Diagnostics

The simplified energy level diagram of Fig. 1a illustrates the basic mechanism of radiative pumping: if a 75  $\mu\text{m}$  photon emitted by dust pumps an ortho-H<sub>2</sub>O molecule from the 2<sub>12</sub> level to the 3<sub>21</sub> one, it can relax via cascade down along the 3<sub>21</sub> → 3<sub>12</sub> → 3<sub>03</sub> → 2<sub>12</sub> ladder through emission in the corresponding 1163, 1097, and 1717 GHz lines. Likewise, a pumping event in the para-H<sub>2</sub>O 2<sub>20</sub> ← 1<sub>11</sub> 101  $\mu\text{m}$  line followed by cascade down along the 2<sub>20</sub> → 2<sub>11</sub> → 2<sub>02</sub> → 1<sub>11</sub> ladder generates H<sub>2</sub>O emission in the 1229, 752, and 988 GHz lines. These can be denoted as “radiative pumping cycles”, and always involve the loss of a continuum photon in the 75 and 101  $\mu\text{m}$  pumping lines. Assuming that the absorption is isotropic, the 75 and 101  $\mu\text{m}$  pumping lines will be seen in absorption. On the other hand, if H<sub>2</sub>O is collisionally excited (e.g. in dense shocks), the 3<sub>21</sub> and 2<sub>20</sub> levels will be populated accordingly and subsequent spontaneous emission in the 3<sub>21</sub> → 2<sub>12</sub> and 2<sub>20</sub> → 1<sub>11</sub> transitions will generate emission, rather than absorption, in both the 75 and 101  $\mu\text{m}$  lines. We can then establish the first qualitative criterion to distinguish between radiative pumping and collisional excitation of the H<sub>2</sub>O submm lines assuming isotropy: in the former case, the 75 and 101  $\mu\text{m}$  lines are expected in absorption, while in the latter case they are expected in emission.

Caveats on the above diagnostic are related to geometry effects. Shock-excited gas could be in front of a strong continuum source that could ultimately generate line absorption at 75 and 101  $\mu\text{m}$  in the direction of the observer. However, since  $T_{\text{gas}}$  and  $n_{\text{H}_2}$ , which determine the excitation in shocks, are fully decoupled from the properties of the continuum source behind (and specifically  $T_{\text{gas}} > T_{\text{dust}}$ ), fine tuning of the shock model would be required to obtain the absorption/emission pattern. On the other hand, lack of absorption in the 75 and 101  $\mu\text{m}$  lines does not fully preclude the radiative pumping mechanism because the responsible far-IR field could be external without impinging on the H<sub>2</sub>O molecules from the back side (in the direction of the observer), and hence would not produce line absorption (Appendix A in González-Alfonso et al. 2014).

A quantitative criterion for radiative pumping arises from statistical equilibrium of the H<sub>2</sub>O levels: since the populations of the 3<sub>21</sub> and 2<sub>20</sub> levels remain constant in time, and assuming that their populations are exclusively determined by the above pumping cycles, the net rate of absorption events in the 3<sub>21</sub> ← 2<sub>12</sub> 75  $\mu\text{m}$  line (hereafter  $R_{75\mu\text{m}}^{\text{abs}}$ ) should be equal to the net rate of emission events in the 3<sub>21</sub> → 3<sub>12</sub> 1163 GHz line

( $R_{1163\text{GHz}}^{\text{ems}}$ ). Likewise, the same equality holds for the para-H<sub>2</sub>O pumping cycle,  $R_{101\mu\text{m}}^{\text{abs}} = R_{1229\text{GHz}}^{\text{ems}}$ . We calculate  $R_{\text{line}}^{\text{ems,abs}}$  in the limit of optically thin continuum emission at 75(101)  $\mu\text{m}$  and isotropic line absorption/emission:

$$R_{\text{line}}^{\text{ems,abs}} (\text{s}^{-1}) = \pm \frac{L_{\text{line}}}{E_{\text{line}}} = \pm 10^{-18} \frac{4\pi D_L^2 F_{\text{line}}}{(1+z)hc} \quad (1)$$

where  $E_{\text{line}} = h\nu_0$  is the energy of line photons,  $D_L$  is the luminosity distance,  $z$  is the redshift,  $h$  is the Planck constant,  $c$  is the speed of light, and  $L_{\text{line}}$  and  $F_{\text{line}}$  are the line luminosity in erg s<sup>-1</sup> and line flux in Jy km s<sup>-1</sup> above (emission, + sign) or below (absorption, – sign) the continuum ( $D_L$ ,  $h$ , and  $c$  are in cgs units).

Equation (1) holds if the H<sub>2</sub>O 75(101)  $\mu\text{m}$  line is optically thick, provided that it remains *effectively* optically thin and repeated absorption/re-emission events in the line end with the photon either escaping from the source (with no contribution to  $R_{\text{line}}^{\text{ems,abs}}$ ) or generating a submm cascade (contributing to both  $R_{\text{line}}^{\text{ems}}$  and  $R_{\text{line}}^{\text{abs}}$ ). However, if the far-IR continuum optical depth becomes significant, thermal continuum photons emitted at 75(101)  $\mu\text{m}$  will have a higher chance, after multiple line absorption/re-emission events, of being absorbed by dust grains before escaping from the source, generating absorption in the far-IR line with no submm line counterpart. In very optically thick regions (with continuum optical depths at 100  $\mu\text{m}$   $\tau_{100} \gg 1$  as found in a number of (U)LIRGs) the emission in the submm lines will be partially extinguished and could even be observed in absorption. As  $\tau_{100}$  increases, additional radiative paths (de)populating the 3<sub>21</sub> and 2<sub>20</sub> levels come into play, but the overall general result is that the absorption fluxes of the 75 and 101  $\mu\text{m}$  surface tracers are increased relative to the emission fluxes of the 1163 and 1229 GHz volume tracers. Therefore, in case of significant far-IR continuum optical depth effects, the  $R_{\text{line}}^{\text{ems,abs}}$  rates calculated in Eq. (1) are only apparent, and we can more generally state that

$$\begin{aligned} R_{75\mu\text{m}}^{\text{abs}} &\geq R_{1163\text{GHz}}^{\text{ems}} \\ R_{101\mu\text{m}}^{\text{abs}} &\geq R_{1229\text{GHz}}^{\text{ems}} \end{aligned} \quad (2)$$

are criteria for the radiative pumping mechanism in isotropic conditions. Anisotropy effects of the exciting radiation field could favor either  $R_{75,101\mu\text{m}}^{\text{abs}}$  or  $R_{1163,1229\text{GHz}}^{\text{ems}}$ , and would spread their relative values for randomly oriented sources.

The “base levels” from which the radiative pumping cycles operate, 2<sub>12</sub> and 1<sub>11</sub>, must still be populated in some way. They could be populated via absorption of dust-emitted photons in the 2<sub>12</sub> ← 1<sub>01</sub> 179  $\mu\text{m}$  and 1<sub>11</sub> ← 0<sub>00</sub> 269  $\mu\text{m}$  ground-state lines, but this mechanism may be inefficient in optically thin  $\tau_{100} < 1$  sources where the dust emission at these wavelengths is weak. At very high redshift, H<sub>2</sub>O excitation from the ground-state can also be produced by the cosmic microwave background (Riechers et al. 2022). Alternatively, the “base levels” could be excited through collisions in warm and dense regions, so that collisional excitation of the low-excitation lines combined with the radiative pumping mechanism would be required to account for the submm emission (González-Alfonso et al. 2014).

## 3. Results

### 3.1. The extragalactic and galactic samples

The crucial diagnostics for distinguishing between radiatively and collisionally excited H<sub>2</sub>O submm emission rely on sensitive observations at 75 and 101  $\mu\text{m}$ . We have applied them to all

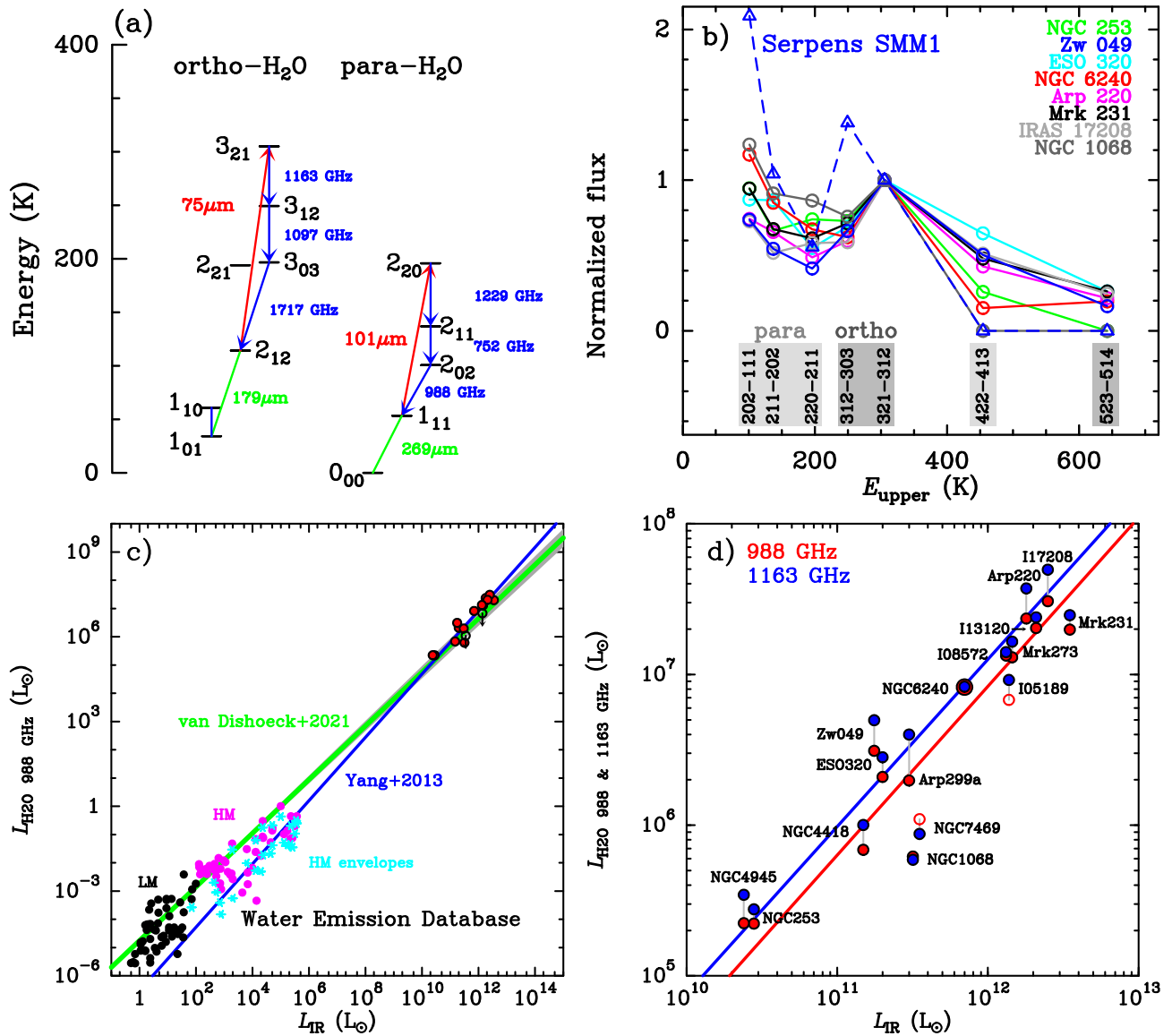


**Fig. 1.** a) A simplified energy level diagram of ortho- and para-H<sub>2</sub>O, illustrating the radiative pumping mechanism of H<sub>2</sub>O submillimeter emission (Sect. 2). b) The Spectral Line Energy Distribution (SLED) of the H<sub>2</sub>O submillimeter lines, normalized to the flux of the 3<sub>21</sub> → 3<sub>12</sub> line, in 8 extragalactic sources where the pumping ortho-H<sub>2</sub>O 3<sub>21</sub> ← 2<sub>12</sub> line at 75 μm has been observed, compared with the SLED in the LMSFR Serpens SMM1 (Goicoechea et al. 2012). The flux of undetected lines is set to 0. c) The luminosity of the H<sub>2</sub>O 2<sub>02</sub> → 1<sub>11</sub> 988 GHz line as a function of the source IR luminosity for both the extragalactic sources considered in this paper (red circles; open circles indicate 3σ upper limits) and the galactic low-mass and high-mass star-forming regions (black and magenta circles, respectively, taken from the Water Emission Database; Dutkowska & Kristensen 2022)<sup>1</sup>. The light-blue symbols isolate the contribution to L<sub>H<sub>2</sub>O 988 GHz</sub> by the envelopes of HMSFRs. The green line shows the best-fit power-law function to all galactic and extragalactic sources found by van Dishoeck et al. (2021), with an index of 0.95 ± 0.02, and the blue line shows the fit found to only (but all) the extragalactic sources by Yang et al. (2013), with an index of 1.12. d) Same as c) but zoomed-in on the extragalactic sources, with the luminosity of the H<sub>2</sub>O 3<sub>21</sub> → 3<sub>12</sub> 1163 GHz line added in blue. The red and blue lines show the fits by Yang et al. (2013).

galaxies that have PACS observations covering the 75 μm line, yielding a sample of 16 sources<sup>2</sup>. Line fluxes and details of the flux derivations will be presented in a forthcoming paper (J. Fischer et al., in prep.). Unfortunately, the PACS gap at ~ 100 μm precluded observations covering the 101 μm line with *Herschel* in all galaxies but Mrk 231 (due to its redshift). This line, however, was detected with *ISO* in Arp 220 (Fischer et al. 2014).

The galactic sample includes 6 well-known HMSFRs where the *Herschel*/PACS and SPIRE observations of the H<sub>2</sub>O 75 μm

<sup>1</sup> <https://katarzynadutkowska.github.io/WED/>

<sup>2</sup> With the exception of M82, which is not detected in the 75 μm nor in the 1163 GHz line, and is therefore excluded from the sample.

and 1163 GHz lines have been carried out: W31C and W49N (Gerin et al. 2015), W51 (Karska et al. 2014a), Sgr B2(M) and (N) (Etxaluze et al. 2013), and the Orion KL outflows (Goicoechea et al. 2015). In addition, the circumnuclear disk (CND) around Sgr A\* (Goicoechea et al. 2013) has been added. The flux of the H<sub>2</sub>O 75 μm line in this sample was extracted from the central 3 × 3 spaxels of PACS (≈ 30'' × 30''). In Orion KL we also measured the line flux in the direction of the Hot Core (hereafter HC, a very bright far-IR continuum source with a size of ~ 10'') within the central spaxel (≈ 10'' × 10''), ‘‘H<sub>2</sub> Peak 1’’ shocked gas position (≈ 30'' × 30''), and Orion KL within a larger field of view (FoV of ≈ 120'' × 120''). The flux of the 1163 GHz

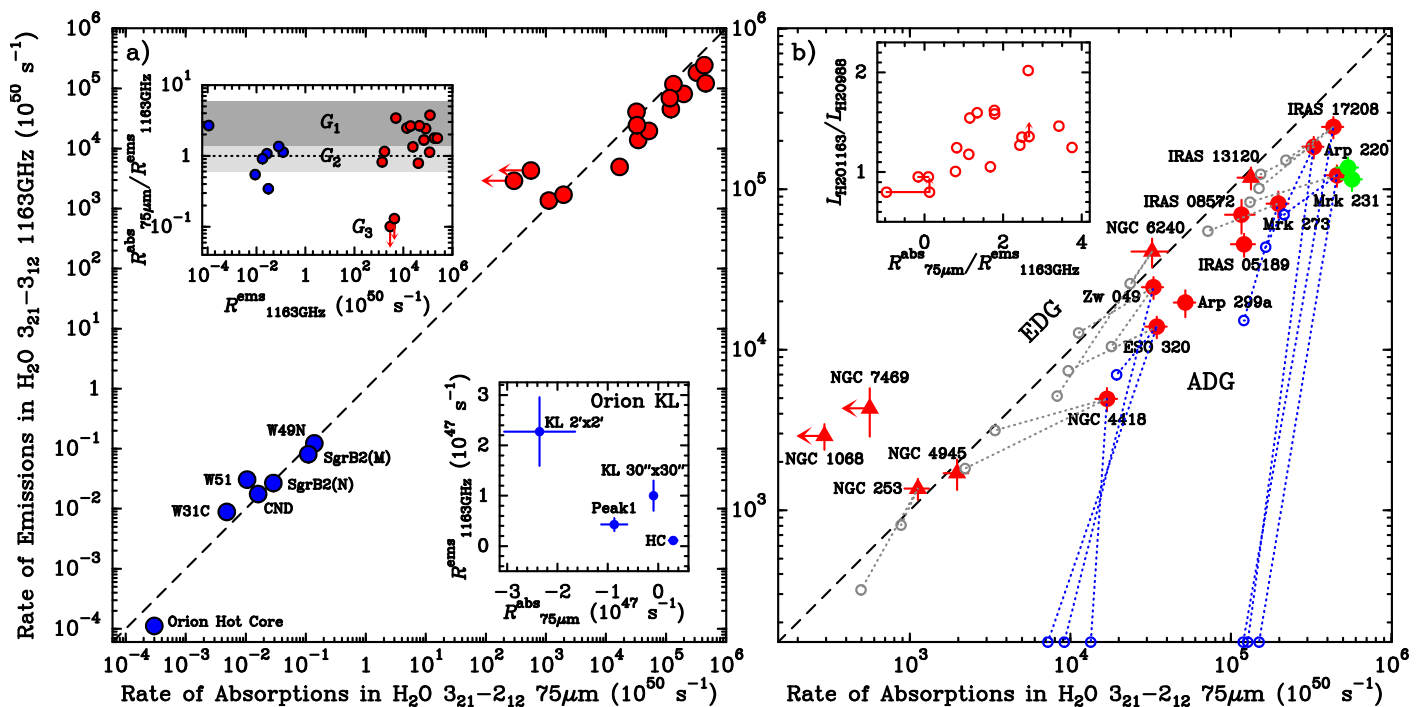


**Fig. 2.** a) The quantitative diagnostic of the radiative pumping mechanism, showing  $R_{1163\text{GHz}}^{\text{ems}}$  as a function of  $R_{75\mu\text{m}}^{\text{abs}}$  for both the galactic and extragalactic samples. The dashed line indicates  $R_{75\mu\text{m}}^{\text{abs}} = R_{1163\text{GHz}}^{\text{ems}}$ . The lower insert shows these values in linear scale for Orion KL, with negative numbers of  $R_{75\mu\text{m}}^{\text{abs}}$  indicating emission in the  $75\mu\text{m}$  line. The upper insert shows  $r \equiv R_{75\mu\text{m}}^{\text{abs}}/R_{1163\text{GHz}}^{\text{ems}}$  versus  $R_{1163\text{GHz}}^{\text{ems}}$ , with shading indicating the  $G_1$ ,  $G_2$ , and  $G_3$  groups defined according to the value of  $r$  (Section 3.3). b) Same as a) but zoomed-in on the extragalactic sources. Circles and triangles indicate ADGs and EDGs, respectively (Section 3.1). The green symbols show the same values but for the  $2_{02} \rightarrow 1_{11}$  (emission) versus the  $2_{20} \leftarrow 1_{11}$  (absorption) in the two sources (Mrk 231 and Arp 220) where the  $101\mu\text{m}$  line has been observed. The open circles show the position in this plane of the optically thin ( $\tau_{100} < 1$ , in gray) and optically thick ( $\tau_{100} > 1$ , in blue) model components used to fit the  $\text{H}_2\text{O}$  emission/absorption (Appendix B). The insert shows the  $3_{21} \rightarrow 3_{12}$ -to- $2_{02} \rightarrow 1_{11}$  luminosity ratio versus  $R_{75\mu\text{m}}^{\text{abs}}/R_{1163\text{GHz}}^{\text{ems}}$ , and horizontal segments indicate the most likely ranges for the 2 sources undetected in  $\text{H}_2\text{O}$   $75\mu\text{m}$ .

line was extracted from similar apertures. The line profiles are displayed in Appendix A.

Our extragalactic sample includes a variety of well-known local (U)LIRGs: a QSO (Mrk 231), AGNs such as IRAS 05189-2524, NGC 1068, NGC 7469, NGC 4945, IRAS 08572+3915, and NGC 6240 (the latter with strong CO emission associated with shocks, see Meijerink et al. 2013), (U)LIRGs with a compact obscured nucleus (NGC 4418, Arp 299a, Zw 049.057, ESO 320-G030, Mrk 273, Arp 220, IRAS 17208-0014), and starburst galaxies (NGC 253 and IRAS 13120-5453). As delineated by the equivalent width of the OH  $65\mu\text{m}$  doublet (Fischer et al. 2014; González-Alfonso et al. 2015), 6 galaxies (NGC 1068, NGC 7469, NGC 253, NGC 6240, IRAS 13120-5453, and NGC 4945) have overall weak far-IR molecular absorption features but usually strong emission in the atomic/ionic fine-structure lines ( $\text{EQW}(\text{OH } 65\mu\text{m}) < 20\text{ km s}^{-1}$ ), and will be referred to as “emission-dominated galaxies” (EDGs), while the rest (with  $\text{EQW}(\text{OH } 65\mu\text{m}) > 20\text{ km s}^{-1}$ ) have stronger far-IR molecular absorption features and will be referred to as “absorption-dominated galaxies” (ADGs).

The extragalactic submm SLEDs, with the  $\text{H}_2\text{O}$  line fluxes normalized to that of the  $3_{21} \rightarrow 3_{12}$   $1163\text{GHz}$  line in Fig. 1b, show a rather common U-shaped pattern for the low-excitation ( $E_{\text{up}} \lesssim 300\text{ K}$ ) lines: the  $1163\text{GHz}$  line is usually the strongest line followed by the  $988\text{GHz}$  line, except in NGC 1068, NGC 6240, and probably NGC 7469 where this sequence is interchanged. This strongly suggests that there is a common dominant excitation mechanism in all sources, but with variations. By contrast, the submm SLED in the LMSFR Serpens SMM1

(a template of collisional excitation in dense shocked gas, e.g. Goicoechea et al. 2012) looks different, with the fluxes of the para- and ortho- lines sharply decreasing with increasing  $E_{\text{up}}$ .

As shown in Fig. 1c, most of the targets lie close to the  $L_{\text{H}_2\text{O}-988\text{GHz}} - L_{\text{IR}}$  correlations found by Yang et al. (2013) (for extragalactic sources) and van Dishoeck et al. (2021) (for both galactic and extragalactic sources), and can thus be considered a representative subsample of (mostly) (U)LIRGs. A closer inspection (Fig. 1d) reveals that NGC 7469 and NGC 1068 have important deficits in the emission of both the  $\text{H}_2\text{O}$   $988\text{GHz}$  ( $2_{02} - 1_{11}$ ) and mostly the  $1163\text{GHz}$  ( $3_{21} - 3_{12}$ ) lines, relative to the best global  $L_{\text{H}_2\text{O}} - L_{\text{IR}}$  fit by Yang et al. (2013), with departures of  $\gtrsim 3$ . Together with NGC 6240, these sources also have the lowest  $1163\text{GHz}/988\text{GHz}$  flux ratio.

### 3.2. The qualitative criterion

Of the 16 galaxies, 14 (87%) show the  $\text{H}_2\text{O}$   $75\mu\text{m}$  far-IR line in absorption (and the  $101\mu\text{m}$  line in Mrk 231 and Arp 220). The other two sources, NGC 1068 and NGC 7469, are ambiguous because the  $75\mu\text{m}$  is not detected at the  $3\sigma$  level. The  $75\mu\text{m}$  spectrum of NGC 1068 is displayed in Appendix C, showing hints of a P Cygni profile that nearly cancels out the blueshifted negative flux and the redshifted positive flux.

In galactic HMSFRs, the  $\text{H}_2\text{O}$   $75\mu\text{m}$  line is observed in absorption in all sources except Orion KL (Fig. A.1). In Orion KL, the nature of the line depends on the specific observed region and FoV: the  $75\mu\text{m}$  line is observed in absorption towards the HC within the central PACS spaxel, but shows a P Cygni profile

or is observed in emission for larger FoVs and towards Peak 1 (Fig. A.1).

By contrast, observations of low-mass Class 0 and I and intermediate mass protostars where H<sub>2</sub>O is collisionally excited in shocks show the H<sub>2</sub>O far-IR lines (including the 75  $\mu$ m line when observed, and with the exception of the 179  $\mu$ m line in some sources) in emission (Herczeg et al. 2012; Goicoechea et al. 2012; Karska et al. 2014b, 2018; Matuszak et al. 2015).

### 3.3. The quantitative criterion

Figure 2a shows  $R_{1163\text{ GHz}}^{\text{ems}}$  as a function of  $R_{75\text{ }\mu\text{m}}^{\text{abs}}$  for both samples, and Figure 2b zooms in on the extragalactic sources. We categorize the galaxies in this plane into 3 groups according to the  $r \equiv R_{75\text{ }\mu\text{m}}^{\text{abs}}/R_{1163\text{ GHz}}^{\text{ems}}$  ratio (see also the upper insert of Fig. 2a):  $G_1$ : 9 galaxies show  $r > 1.4$ ;  $G_2$ : 5 sources lie close, within the calibration uncertainties, to the  $R_{75\text{ }\mu\text{m}}^{\text{abs}} = R_{1163\text{ GHz}}^{\text{ems}}$  line ( $0.6 < r < 1.4$ );  $G_3$ : 2 galaxies, NGC 1068 and NGC 7469, have only upper limits in  $R_{75\text{ }\mu\text{m}}^{\text{abs}}$  and show much higher  $R_{1163\text{ GHz}}^{\text{ems}}$ . With the exception of Zw 049.057, all ADGs belong to  $G_1$ , so that the plane of Fig. 2 can be used to discriminate between ADGs and EDGs from the observation of only two lines. On the other hand, most of the galactic HMSFRs of our sample except Orion KL lie close to the  $R_{75\text{ }\mu\text{m}}^{\text{abs}}/R_{1163\text{ GHz}}^{\text{ems}} = 1$  line, with values ranging from 0.34 (W51) to 1.4 (SgrB2(M)), and can thus be classified as belonging to  $G_2$ . Orion HC shows an excess of  $R_{75\text{ }\mu\text{m}}^{\text{abs}}$  similar to  $G_1$  sources, but once the FoV increases (KL 30''  $\times$  30'' and 2'  $\times$  2') or towards Peak 1,  $R_{75\text{ }\mu\text{m}}^{\text{abs}}$  becomes negative (i.e. it is observed in emission, lower insert in Fig 2a).

Overall, most of the (U)LIRGs and HMSFRs observed in the H<sub>2</sub>O 75  $\mu$ m line (nearly) follow the prediction of Eq. (2) over 9 orders of magnitude in  $R_{1163\text{ GHz}}^{\text{ems}}$ , indicating that far-IR pumping is the essential ingredient to understand the H<sub>2</sub>O submm emission and specifically it dominates the observed H<sub>2</sub>O 3<sub>21</sub> – 3<sub>12</sub> 1163 GHz emission (and thus also the 3<sub>12</sub> – 3<sub>03</sub> 1097 GHz emission) in the bulk of sources. In some galaxies and HMSFRs, there is an excess of submm emission over far-IR absorption ( $R_{75\text{ }\mu\text{m}}^{\text{abs}}/R_{1163\text{ GHz}}^{\text{ems}} = 0.34 - 1$ ), which could reflect either a contribution to the submm line flux by shock-excited H<sub>2</sub>O or specific geometrical effects.

Multicomponent model fits to the emission/absorption fluxes of both the SPIRE and the PACS H<sub>2</sub>O lines, and including the far-IR spectral energy distribution (SED), have been performed for most galaxies of our sample following the approach described in González-Alfonso et al. (2021) (these will be presented in a forthcoming paper). Classifying the best-fit model components of each galaxy as “optically thin” if the optical depth of the continuum at 100  $\mu$ m is lower than 1 ( $\tau_{100} < 1$ ), and “optically thick” if  $\tau_{100} \geq 1$ , Fig. 2b shows that the  $\tau_{100} < 1$  components (in gray) lie close to the  $R_{75\text{ }\mu\text{m}}^{\text{abs}} = R_{1163\text{ GHz}}^{\text{ems}}$  line as expected, while the optically thick components (in blue) predict weak emission in the 1163 GHz line, and even in some extreme nuclei in absorption. The ADGs have  $R_{75\text{ }\mu\text{m}}^{\text{abs}} > R_{1163\text{ GHz}}^{\text{ems}}$  because of the presence of buried components that generate strong absorption in the H<sub>2</sub>O 75  $\mu$ m but little emission in the submm lines due to high continuum brightness and extinction in the submm. The submm lines are in contrast formed in optically thin/moderately thick and more extended regions, likely the 0.1 – 0.5 kpc circumnuclear disks of (U)LIRGs.

In Appendix B we compare the observed submm SLEDs of 8 sample galaxies and the best-fit predictions by the multicomponent models, generally showing good agreement with a

minimum emission line flux in the 2<sub>20</sub> – 2<sub>11</sub> 1229 GHz line. We also show that in some EDGs (NGC 6240 and NGC 253) collisional excitation of the base levels is required to make the radiative pumping operational, and finally discuss in Appendix C whether the cases of NGC 7469 and NGC 1068 represent sources where H<sub>2</sub>O is shock-excited, or whether geometrical effects can account for the lack of H<sub>2</sub>O 75  $\mu$ m absorption.

## 4. Discussion and conclusions

The preponderance of H<sub>2</sub>O 75  $\mu$ m absorption is difficult to reconcile with collisional excitation in shock cavities devoid of significant amounts of warm dust. An alternative is to assume that the H<sub>2</sub>O 1163 GHz line is generated in an ensemble of shock cavities, where the H<sub>2</sub>O 75  $\mu$ m line is also generated in emission, while a spatially separated and unrelated  $\tau_{100} \gg 1$  component produces the 75  $\mu$ m absorption (almost always stronger than the emission to generate net absorption in the line). However, this scenario does not explain the correlation between  $R_{75\text{ }\mu\text{m}}^{\text{abs}}$  and  $R_{1163\text{ GHz}}^{\text{ems}}$  as the two lines are generated in different regions and by different mechanisms. Even if  $\dot{E}$  (mechanical) and  $L_{\text{IR}}$  are related, the specific lines respond in different ways to the far-IR and mechanical feedback. The case of Orion KL illustrates this point: large FoVs show emission in the 75  $\mu$ m line far above the absorption towards the HC (lower insert in Fig. 2a).

The following interpretation of the  $L_{\text{H}_2\text{O } 988\text{ GHz}} - L_{\text{IR}}$  correlation stems from the present analysis. In Fig. 1c, we have increased the dynamic range of the correlation found by Yang et al. (2013) for extragalactic sources to the luminosities characteristic of galactic sources, assuming that the “radiative pumping slope” of 1.12 holds. Then, a number of HMSFRs and basically all LMSFRs, where H<sub>2</sub>O is shock-excited, lie well above this line. Using the spectral decomposition of the H<sub>2</sub>O 988 GHz spectra in HMSFRs carried out by van der Tak et al. (2013) and San José-García et al. (2016), we have plotted in Fig. 1c the H<sub>2</sub>O 988 GHz luminosities due to only the massive envelopes of HMSFRs (light-blue symbols), finding a good match with the extended extragalactic correlation. We thus propose that these galactic massive envelopes play a role similar to the circumnuclear disks in galaxies (including the CNB of the Milky Way), where the H<sub>2</sub>O submm emission is radiatively pumped<sup>3</sup> -combined at least in some cases with collisional excitation of the low-energy levels. Galactic sources located significantly above the blue line in Fig. 1c would indicate dominance of excitation by shocks. The location of the galactic HMSFRs in Fig. 2a resemble the starburst galaxies NGC 253 and IRAS 13120-5453, lacking an obscured nucleus that in its prominent form is a unique feature of extragalactic sources.

While we expect that the para-H<sub>2</sub>O 101  $\mu$ m pumping cycle is as important as the ortho-H<sub>2</sub>O 75  $\mu$ m one, the low-excitation 1<sub>11</sub> and 2<sub>02</sub> levels will be more affected by collisions in warm/dense regions than the 3<sub>21</sub> one; therefore the 988 GHz line has less ability than the 1163 GHz line to discriminate between the two mechanisms.

*Acknowledgements.* We thank the referee for helpful comments that improved the clarity of the manuscript. EG-A is a Research Associate at the Harvard-Smithsonian Center for Astrophysics, and thanks the Spanish MICINN for support under project PID2019-105552RB-C41. JRG thanks the Spanish MCINN for funding support under grant PID2019-106110GB-I00. JF and KPS gratefully acknowledge support through NASA grant NNN17ZD001N-ADAP. C.Y.

<sup>3</sup> In this framework, the slope of 1.1 could be due to the increasing linewidth  $\Delta\nu$  with  $L_{\text{IR}}$ , as for the optically thick 75 and 101  $\mu$ m lines  $R_{75-101\text{ }\mu\text{m}}^{\text{abs}} \propto \Delta\nu$ . If  $\Delta\nu$  increases by a factor  $\sim 5$  as  $L_{\text{IR}}$  increases by 7 dex, the index of the correlation will be  $\sim 1 + (\log_{10} 5)/7 = 1.1$ .

acknowledges support from ERC Advanced Grant 789410. MPS acknowledges support from the Comunidad de Madrid through the Atracción de Talento Investigador Grant 2018-T1/TIC-11035 and PID2019-105423GA-I00 (MCIU/AEI/FEDER,UE). PACS was developed by a consortium of institutes led by MPE (Germany) and including UVIE (Austria); KU Leuven, CSL, IMEC (Belgium); CEA, LAM (France); MPIA (Germany); INAF/IFSI/OAA/OAP/OAT, LENS, SISSA (Italy); IAC (Spain). This development has been supported by the funding agencies BMVIT (Austria), ESA-PRODEX (Belgium), CEA/CNES (France), DLR (Germany), ASI/INAF (Italy), and CICYT/MCYT (Spain). SPIRE was developed by a consortium of institutes led by Cardiff University (UK) and including Univ. Lethbridge (Canada); NAOC (China); CEA, LAM (France); IFSI, Univ. Padua (Italy); IAC (Spain); Stockholm Observatory (Sweden); Imperial College London, RAL, UCL-MSSL, UKATC, Univ. Sussex (UK); and Caltech, JPL, NHSC, Univ. Colorado (USA). This development has been supported by national funding agencies: CSA (Canada); NAOC (China); CEA, CNES, CNRS (France); ASI (Italy); MCINN (Spain); SNSB (Sweden); STFC, UKSA (UK); and NASA (USA).

## References

- Cernicharo, J., Goicoechea, J. R., Daniel, F., et al. 2006, *ApJ*, 649, L33
- de Graauw, T., Helmich, F. P., Phillips, T. G., et al. 2010, *A&A*, 518, L6
- Dutkowska, K. M. & Kristensen, L. E. 2022, arXiv e-prints, arXiv:2206.01753
- Etzaluze, M., Goicoechea, J. R., Cernicharo, J., et al. 2013, *A&A*, 556, A137
- Falstad, N., González-Alfonso, E., Aalto, S., & Fischer, J. 2017, *A&A*, 597, A105
- Falstad, N., González-Alfonso, E., Aalto, S., et al. 2015, *A&A*, 580, A52
- Fischer, J., Abel, N. P., González-Alfonso, E., et al. 2014, *ApJ*, 795, 117
- Gerin, M., Ruaud, M., Goicoechea, J. R., et al. 2015, *A&A*, 573, A30
- Goicoechea, J. R., Cernicharo, J., Karska, A., et al. 2012, *A&A*, 548, A77
- Goicoechea, J. R., Chavarría, L., Cernicharo, J., et al. 2015, *ApJ*, 799, 102
- Goicoechea, J. R., Etzaluze, M., Cernicharo, J., et al. 2013, *ApJ*, 769, L13
- González-Alfonso, E., Fischer, J., Aalto, S., & Falstad, N. 2014, *A&A*, 567, A91
- González-Alfonso, E., Fischer, J., Isaak, K., et al. 2010, *A&A*, 518, L43
- González-Alfonso, E., Fischer, J., Sturm, E., et al. 2015, *ApJ*, 800, 69
- González-Alfonso, E., Pereira-Santaella, M., Fischer, J., et al. 2021, *A&A*, 645, A49
- Griffin, M. J., Abergel, A., Abreu, A., et al. 2010, *A&A*, 518, L3
- Hailey-Dunsheath, S., Sturm, E., Fischer, J., et al. 2012, *ApJ*, 755, 57
- Herczeg, G. J., Karska, A., Bruderer, S., et al. 2012, *A&A*, 540, A84
- Karska, A., Herpin, F., Bruderer, S., et al. 2014a, *A&A*, 562, A45
- Karska, A., Kaufman, M. J., Kristensen, L. E., et al. 2018, *ApJS*, 235, 30
- Karska, A., Kristensen, L. E., van Dishoeck, E. F., et al. 2014b, *A&A*, 572, A9
- Kessler, M. F., Steinz, J. A., Anderegg, M. E., et al. 1996, *A&A*, 315, L27
- Kristensen, L. E., van Dishoeck, E. F., Bergin, E. A., et al. 2012, *A&A*, 542, A8
- Liu, L., Weiß, A., Perez-Beaupuits, J. P., et al. 2017, *ApJ*, 846, 5
- Lu, N., Zhao, Y., Diaz-Santos, T., et al. 2017, *VizieR Online Data Catalog*, J/ApJS/230/1
- Matuszak, M., Karska, A., Kristensen, L. E., et al. 2015, *A&A*, 578, A20
- Meijerink, R., Kristensen, L. E., Weiß, A., et al. 2013, *ApJ*, 762, L16
- Omont, A., Neri, R., Cox, P., et al. 2011, *A&A*, 530, L3
- Omont, A., Yang, C., Cox, P., et al. 2013, *A&A*, 551, A115
- Pereira-Santaella, M., González-Alfonso, E., Usero, A., et al. 2017, *A&A*, 601, L3
- Pilbratt, G. L., Riedinger, J. R., Passvogel, T., et al. 2010, *A&A*, 518, L1
- Poglitsch, A., Waelkens, C., Geis, N., et al. 2010, *A&A*, 518, L2
- Riechers, D. A., Weiss, A., Walter, F., et al. 2022, *Nature*, 602, 58
- San José-García, I., Mottram, J. C., van Dishoeck, E. F., et al. 2016, *A&A*, 585, A103
- Spinoglio, L., Pereira-Santaella, M., Busquet, G., et al. 2012, *ApJ*, 758, 108
- van der Tak, F. F. S., Chavarría, L., Herpin, F., et al. 2013, *A&A*, 554, A83
- van der Werf, P. P., Berciano Alba, A., Spaans, M., et al. 2011, *ApJ*, 741, L38
- van der Werf, P. P., Isaak, K. G., Meijerink, R., et al. 2010, *A&A*, 518, L42
- van Dishoeck, E. F., Kristensen, L. E., Mottram, J. C., et al. 2021, *A&A*, 648, A24
- Yang, C., Gao, Y., Omont, A., et al. 2013, *ApJ*, 771, L24
- Yang, C., Gavazzi, R., Beelen, A., et al. 2019, *A&A*, 624, A138
- Yang, C., Omont, A., Beelen, A., et al. 2016, *A&A*, 595, A80

## Appendix A: The H<sub>2</sub>O 75 $\mu$ m profiles in galactic high-mass star-forming regions

Figure A.1 shows the H<sub>2</sub>O 75  $\mu$ m and 1163 GHz profiles in our sample of galactic high-mass star-forming regions.

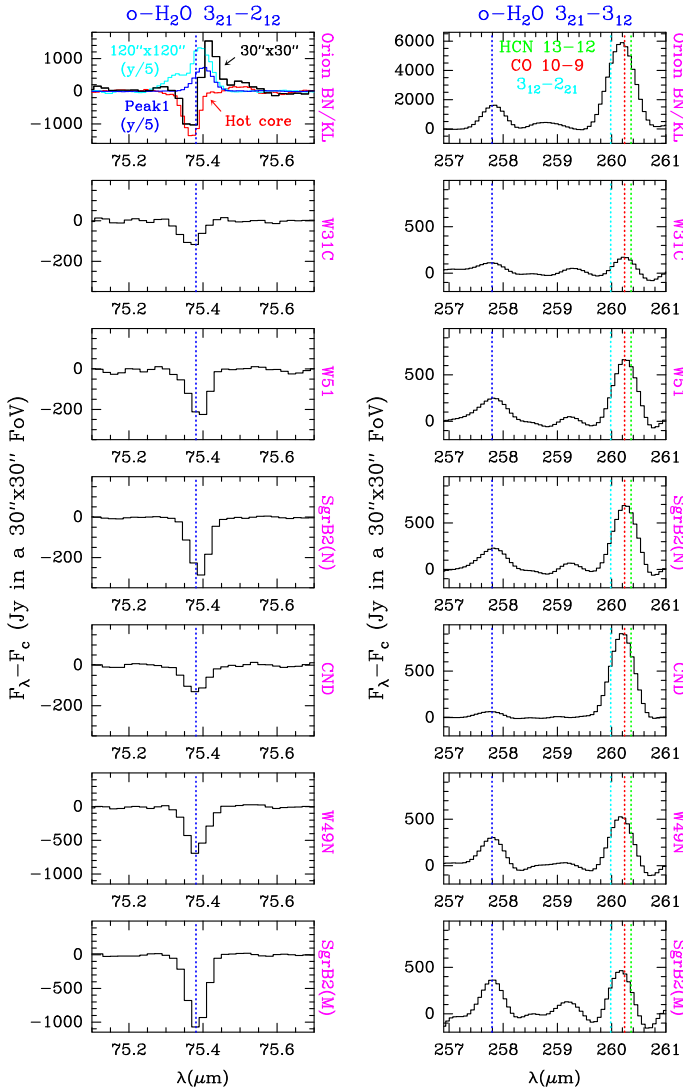


**Fig. A.1.** The H<sub>2</sub>O 3<sub>21</sub> – 2<sub>12</sub> 75  $\mu$ m (left) and H<sub>2</sub>O 3<sub>21</sub> – 3<sub>12</sub> 1163 GHz (right) profiles in 7 galactic high-mass star-forming regions, as observed with *Herschel*/PACS and SPIRE. The apodized SPIRE profiles also include the blend of CO 10–9 (which dominates the observed emission), H<sub>2</sub>O 3<sub>12</sub> – 2<sub>21</sub>, and HCN 13–12. The PACS spectra correspond to the central 3  $\times$  3 spaxels ( $\approx$  30''  $\times$  30''). In Orion KL, the H<sub>2</sub>O 75  $\mu$ m line is observed in absorption towards the Hot Core as seen within the central PACS spaxel ( $\approx$  10''  $\times$  10''), but shows P Cygni and emission profiles for larger field-of-views and towards Peak 1 (upper-left panel; see also the insert in Fig. 2a).

## Appendix B: The submillimeter SLEDs

Figure B.1a compares the observed submm SLEDs with the best-fit predictions (in red) by the multicomponent models applied to 8 sample galaxies, 4 (sub)LIRGs and 4 ULIRGs (see also Falstad et al. 2015, 2017, for similar models applied to Zw 049-057 and Arp 299a). In these models, collisional excitation was only roughly simulated with a single value of  $T_{\text{gas}} = 150$  K and 3 values of the density ( $n(\text{H}_2)$ ):  $1.7 \times 10^4$ ,  $5 \times 10^4$ , and

$1.5 \times 10^5$  cm<sup>-3</sup> (González-Alfonso et al. 2021). Only in the case of NGC 6240, the highest density was favored for the component that dominates the H<sub>2</sub>O submm emission. Although with some discrepancies, the overall SLEDs are naturally reproduced with far-IR radiation fields that also account for the PACS lines and the SED.

For the model components in Fig. B.1a, we use the same nomenclature as in González-Alfonso et al. (2021): blue, green, and gray circles indicate the contributions to the model fit by the “core”, “disk”, and “envelope” components, respectively, and red is total. Schematically, the high-excitation absorption lines are formed in the far-IR photosphere of the optically thick and very warm cores; the medium-excitation absorption and emission lines have contributions from the disk components, and the envelopes dominate the H<sub>2</sub>O submm line emission and also generate some absorption in the low-excitation far-IR lines (such as the 75  $\mu$ m line).

A general characteristic of the H<sub>2</sub>O submm SLEDs of galaxies is their *U*-shape, shown also in Fig. 1b. It is instructive to understand that, according to our non-local models, the minimum emission line flux in most cases, which corresponds to the para-H<sub>2</sub>O 2<sub>20</sub> – 2<sub>11</sub> 1229 GHz line, is due to competing *absorption* of the continuum by the line in the optically thicker core and disk components, rather than an intrinsic weakness of the 1229 GHz line emission from the optically thin envelope. The main reason that the absorption in the 1229 GHz line is the strongest is that it has an  $A_{ul}$ –Einstein coefficient 2.7 $\times$  higher than that of the 2<sub>11</sub> – 2<sub>02</sub> 752 GHz line. Close to the source surface, this has the effect of reducing the excitation temperature ( $T_{\text{ex}}$ ) of the 1229 GHz line, which will be thus more prone to absorb the brighter (due to its also higher frequency) continuum behind. The same effect does not occur with the ortho-H<sub>2</sub>O 3<sub>21</sub> – 3<sub>12</sub> 1163 GHz line, because its  $A_{ul}$  is only 1.2 $\times$  higher than  $A_{ul}(3_{12} - 3_{03}) + A_{ul}(3_{12} - 2_{21})$ , and thus the 1163 GHz line remains relatively excited (and even with supra-thermal excitation in some models) close to the surface. The described absorption effect specific to the 1229 GHz line in ADGs is indeed clearly seen in our data: in Fig. 1b, Arp 220 (with a prominent core) shows one of the lowest (relative) 1229 GHz fluxes, while the EDGs NGC 1068 and NGC 253 do not show that dip. In summary, while the flux of the H<sub>2</sub>O submm emission is dominated by the envelopes, the cores and disks modulate the line ratios generating the SLED *U*-shaped pattern.

In contrast with the nearly flat submm SLEDs for the envelopes predicted by the radiative pumping scenario (in absence of important collisional excitation of the low-excitation lines, see below), the SLED of Serpens SMM1<sup>4</sup> shows a strong decline of the fluxes of the para- and ortho- lines with increasing  $E_{\text{up}}$  (Fig. 1b). Here, the dip in the para-H<sub>2</sub>O 2<sub>20</sub> – 2<sub>11</sub> 1229 GHz line has nothing to do with the absorption of any continuum, but with the difficulty of exciting the 2<sub>20</sub> level without a continuum source emitting at 101  $\mu$ m. A characteristic of H<sub>2</sub>O shock excitation in dense gas is that the ortho 3<sub>12</sub> – 3<sub>03</sub> 1097 GHz line is expected to be stronger than the 3<sub>21</sub> – 3<sub>12</sub> 1163 GHz line, as opposed to the situation when radiative pumping dominates.

For each of the 8 sources, Fig. B.1b shows the predictions for only the envelope component that dominates the H<sub>2</sub>O submm emission (gray symbols). To better understand the relative roles

<sup>4</sup> The Serpens SMM1 line fluxes were taken from Table A.1 of Goicoechea et al. (2012), with the exception of a few fluxes that appeared with typographical errors. The H<sub>2</sub>O 2<sub>20</sub> – 2<sub>11</sub> and 2<sub>21</sub> – 1<sub>10</sub> lines should have been listed as  $1.46 \times 10^{-16}$  and  $1.35 \times 10^{-15}$  W m<sup>-2</sup> instead of  $2.92 \times 10^{-17}$  and  $1.35 \times 10^{-16}$  W m<sup>-2</sup>, respectively.

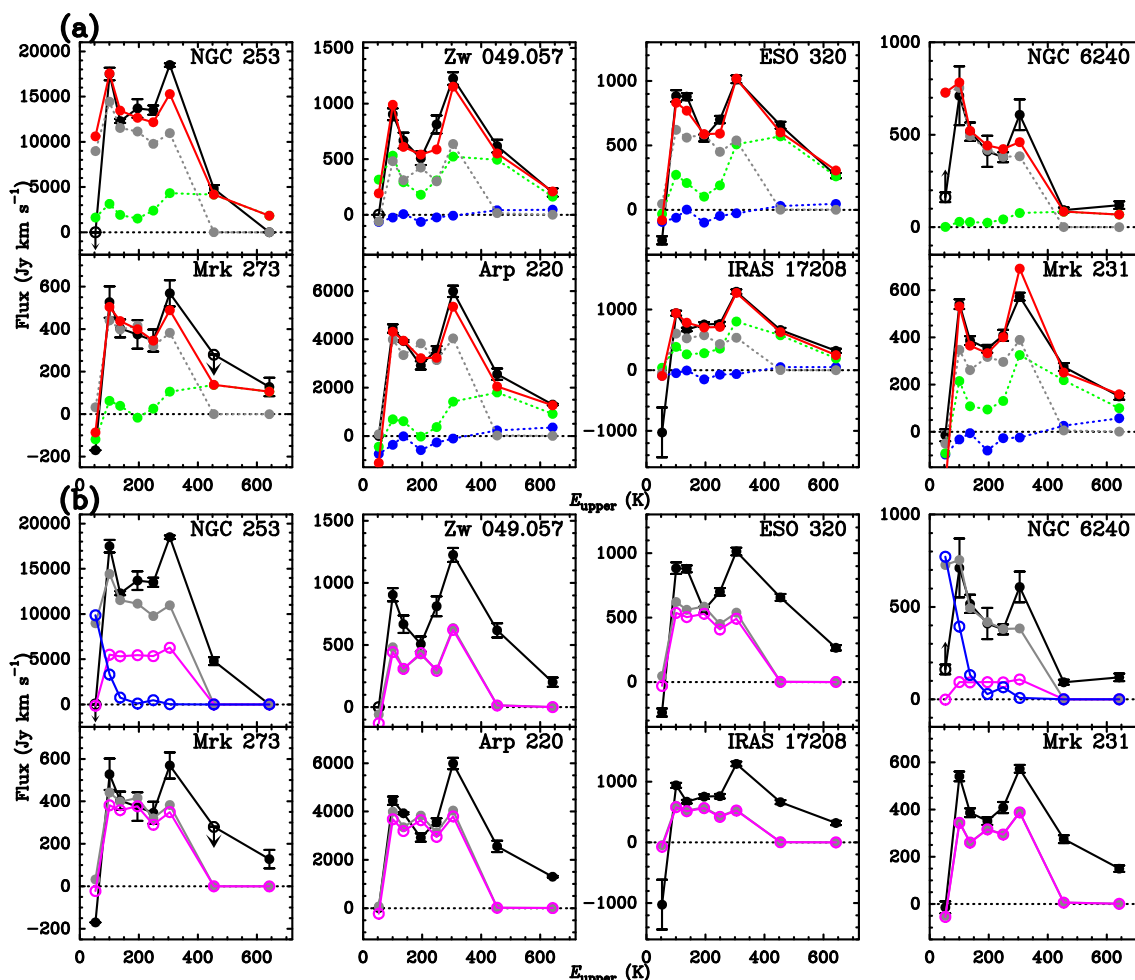


**Fig. B.1.** a) Fits to the H<sub>2</sub>O submillimeter emission for 8 local extragalactic sources analyzed in this paper, including all modeling components. Black circles with errorbars show the observed fluxes. Blue, green, and gray circles indicate the contributions to the model fit by the core, disk, and envelope components, respectively, and red is total. b) The model component that dominates the emission of the H<sub>2</sub>O low-excitation submillimeter lines (the envelope component) is shown with gray circles and lines. For comparison, magenta symbols and lines show the modeling results for these components obtained when the collisional excitation is quenched, and blue symbols (for NGC 253 and NGC 6240) indicate the results obtained when the far-IR pumping is quenched (but collisional excitation is included).

of collisional and radiative pumping, we have generated exactly the same models but quenching the collisional rates (in magenta). While in the 4 ULIRGs results remain the same, meaning that collisional excitation has little effect on the H<sub>2</sub>O excitation, the quenching of collisions has a strong effect in some sub-ULIRGs, specifically in NGC 253 and NGC 6240. In these EDGs, we also generated the same models but quenching the pumping radiation field and keeping the collisional excitation (in blue), with the result that the line fluxes dropped dramatically for all except the  $1_{11} - 0_{00}$  and  $2_{02} - 1_{11}$  lines. This indicates that collisional excitation is required to populate the “base levels” ( $2_{12}$  and  $1_{11}$ ) from which the pumping cycles operate (González-Alfonso et al. 2014). In these sources, it is the combination of collisional excitation of the base levels and radiative pumping from them that generates the H<sub>2</sub>O submm emission. These results also suggest that in the highest luminosity galaxies, collisional excitation of the base levels tends to be less important.

### Appendix C: Outliers (NGC 1068 and NGC 7469): collisional excitation or geometrical effects?

NGC 1068 and NGC 7469 are ambiguous sources, because the H<sub>2</sub>O 75  $\mu$ m line is neither detected in absorption, as expected in

the scenario of radiative pumping, nor in emission, as expected in case of shock excitation. As shown in Fig. 1d, both sources are underluminous in both H<sub>2</sub>O 1163 GHz and 988 GHz lines relative to  $L_{\text{IR}}$ , with a stronger deficit in the 1163 GHz line. These galaxies are thus not representative of the bulk of (U)LIRGs observed with SPIRE and fitted by Yang et al. (2013), but may well represent a population of low-luminosity AGNs ( $\lesssim 10^{11} L_{\odot}$ ) with starburst rings under-sampled by *Herschel*/PACS and SPIRE.

The PACS continuum-subtracted spectra around the H<sub>2</sub>O  $3_{21} - 2_{12}$  75  $\mu$ m line in NGC 1068 and NGC 7469 are shown in Fig. C.1. The net flux of the line in both sources is below  $3\sigma$  ( $42 \pm 64$  and  $73 \pm 30$  Jy km s<sup>-1</sup>), but hints of a P Cygni profile are seen in the spectrum of NGC 1068 with the absorption and emission features nearly cancelling each other. P Cygni profiles with similar absorption and emission fluxes are characteristic of radiatively excited lines. We note that the redshifted emission component will also contribute to the 1163 GHz flux via radiative pumping without generating 75  $\mu$ m absorption because the emitting gas is behind the continuum source. This is one example of anisotropy alluded to in Section 2. However, the measured flux in the 75  $\mu$ m blueshifted absorption component falls too short to account for the observed strong submm emission in the 1163 GHz line.



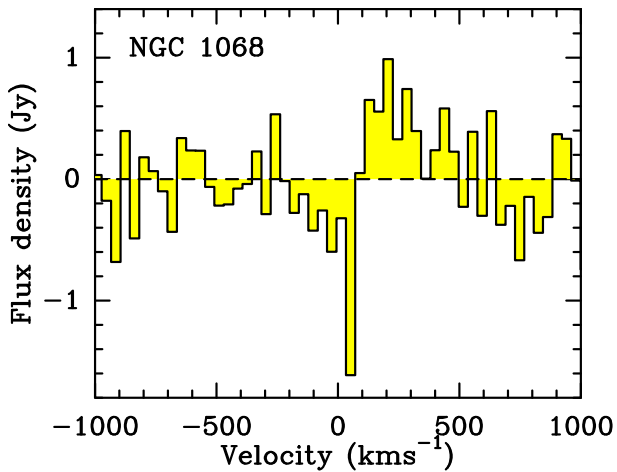


**Fig. C.1.** The H<sub>2</sub>O  $3_{21} - 2_{12}$   $75\ \mu\text{m}$  continuum-subtracted spectrum in NGC 1068.

Spinoglio et al. (2012) reported and analyzed the H<sub>2</sub>O submm emission in NGC 1068, including the detected PACS lines (all in emission). The H<sub>2</sub>O emission was found to be dominated by the CNB around the AGN. Collisional excitation of H<sub>2</sub>O is important in the CNB, as indicated by e.g. the relatively strong emission of the H<sub>2</sub>O  $1_{11} - 0_{00}$  1113 GHz line, and by a 1163-to-988 flux ratio lower than 1 (Fig. 1b). However, the proposed LVG models that ignored radiative pumping yielded  $T_{\text{gas}} \sim 40$  K for the H<sub>2</sub>O in the CNB that did not match the conditions inferred from the CO lines ( $T_{\text{gas}} \sim 170 - 570$  K, Hailey-Dunsheath et al. 2012). An alternative model was then explored by González-Alfonso et al. (2014), which included the radiative pumping effect by the dust mixed with H<sub>2</sub>O and also by an external far-IR radiation field that was anisotropic, that is, it did not impinge onto the clumps in the direction of the observer and thus did not produce absorption of the far-IR lines in the direction of the Earth. On the contrary, the external field produced emission in the far-IR lines, which would nearly cancel the absorption by the internal field in the case of the  $75\ \mu\text{m}$  line. A similar situation could take place in the Sy 1.2 galaxy NGC 7469.